Forward Blade Sweep Applied to Low-Speed Axial Fan Rotors of Controlled Vortex Design: An Overview

János Vad
Department of Fluid Mechanics,
Budapest University of
Technology and Economics,
Bertalan Lajos u. 4–6,
H-1111 Budapest, Hungary

An overview is given on the research maintained by the author about the design aspects of three-dimensional blade passage flow in low-speed axial flow industrial fan rotors, affected by spanwise changing design blade circulation due to controlled vortex design (CVD), blade forward sweep (FSW), and their combination. It was pointed out that, comparing the CVD method to the free vortex design, the fluid in the blade suction side boundary layer has an increased inclination to migrate radially outward, increasing the near-tip blockage and loss. It was concluded that the benefit of FSW, in terms of moderating loss near the tip, can be better utilized for the rotors of the CVD, in comparison to the free vortex design. Compared to the free vortex design, the FSW applied to the blades of the CVD was found to also be especially beneficial in loss reduction away from the endwalls, via shortening the flow paths on the suction side—in any case being elongated by the radially outward flow due to CVD—and thus, reducing the effect of wall skin friction. The necessity of correcting the swept blades was pointed out for matching with the prescribed CVD circulation distribution. [DOI: 10.1115/1.4007428]

Keywords: axial flow fan rotor, controlled vortex design, blade sweep

Introduction

In the classic free vortex design (FVD) of axial flow rotor blade rows, a spanwise constant blade circulation is prescribed. As an alternative to the FVD method, the controlled vortex design (CVD) concept is widely used at present. In the CVD, the blade circulation and the isentropic total pressure rise increases along the blade span in a prescribed manner. The major benefits of the CVD are summarized as follows. The CVD enhances the contribution of blade sections at higher radii to the rotor performance, offering the potential for the realization of rotors of relatively high specific performance; see, e.g., Refs.[1,2]: a relatively high flow rate and/or total pressure rise can be obtained with moderate diameter and rotor speed (e.g., Φ_D and Ψ_D up to 0.6 and 0.8, respectively, in Ref. [2]), and with a moderate blade count. Moderate loading can be prescribed for the blade root, providing a means for hub loss reduction; see, e.g., Refs. [2–5]. The CVD serves as the conceptual basis for the obtainment of easy-to-manufacture blade geometry, e.g., by avoiding highly twisted blades; see, e.g., Refs. [3–6]. In multistage machinery, the CVD represents a strategy for realizing a rotor exit flow angle distribution that is appropriate for the inlet to the consecutive stage; see, e.g., Refs. [7,8]. Besides the aforementioned favorable features, the vortices shed from the CVD blade of the spanwise changing circulation are associated with three-dimensional (3D) flow phenomena in the blade passage, introducing difficulties in blade design and in the judgment of loss-generating mechanisms.

For a quantification of the intensity of the radial change of the isentropic total pressure rise in the CVD concept, a spanwise-mean representative data of $d\psi_D/dR$ is introduced herein.

A blade is swept when the cylindrical sections of a datum—"unswept" (USW)—blade of the radial stacking line are shifted parallel to their chord. Forward sweep (FSW) means that, considering the relative flow field, the blade section at a given radius is upstream of the neighboring section at a lower radius. The FSW is often incorporated in the circumferential forward skew (FSK), for which the datum blade sections are shifted in the circumferential direction, towards the direction of rotation. As overviewed in [9], the FSW offers an increased capability for the performance and efficiency improvement via controlling the 3D blade passage flow.

For a quantification of the FSW, the sweep angle λ is introduced herein as the angle between (i) the radial direction, and (ii) the projection of the stacking line to the plane determined by the chordline and the radial direction [9].

The CVD and FSW are often applied together, aiming at combining the aforementioned benefits. For illustrative examples, Fig. 1 presents the CVD fan rotors featuring the FSW or the FSK, designed by the author with a consideration of guidelines presented in the paper. The types and blade tip diameters of the rotors presented in the figure are as follows: (a) Electric motor cooling fans, FSK blades, Ø 110 mm, Ø 124 mm [10], (b) a high-performance axial fan for industrial purposes, FSW blades, Ø 630 mm [1], and (c) a wind tunnel fan, FSK blades, Ø 2000 mm [11].

Both the CVD and the FSW influence the 3D interblade flow. Still, the effects of sweep are often presented in the literature as features being independent from the fact that the blading has been designed for spanwise increasing circulation; see, e.g., [4,6–8,12–15]. Only a very few papers comment on the *combined* effects of the CVD and FSW [1,16]. This paper aims at extending the knowledge on the design aspects of CVD, FSW, and their combination, in terms of 3D flow phenomena developing in the blade passages. For this reason, the results of a related long-term research program, maintained by the author, are overviewed in a

Contributed by the International Gas Turbine Institute (IGTI) of ASME for publication in the Journal of Engineering for Gas Turbines and Power. Manuscript received June 16, 2012; final manuscript received July 12, 2012; published online November 21, 2012. Editor: Dilip R. Ballal.

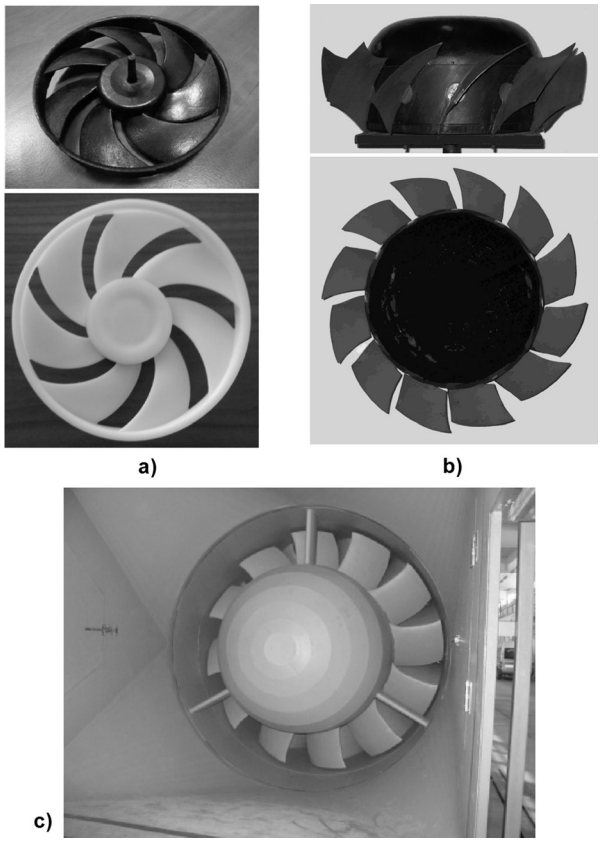

Fig. 1 Fan rotors of the CVD and the FSW/FSK

comprehensive manner. Isolated axial fan rotors, or rotors without an inlet guide vane but followed by a stator, are considered. Low-speed fan rotors are discussed, presuming incompressible flow. The discussion is confined to the design flow rate.

Near-Tip Blockage and Loss

The studies regarding the effects of the CVD design style on near-tip blockage and total pressure loss, along with their influence by the FSW, have been reported in [17] and are outlined in this section.

Due to the spanwise blade circulation gradient, represented quantitatively by $d\psi_D/dR > 0$*, vortices are shed from the CVD blade. These shed vortices are associated with radial outward and inward flows on the blade suction side (SS) and pressure side, respectively*. As a consequence, a characteristic 3D flow pattern develops in the CVD blade passage. The development of a 3D blade passage flow is illustrated in Fig. 2 in the computational fluid dynamics (CFD) example (in Ref. [17], based on Ref. [18]).

It is known that the fluid in the SS boundary layer (BL) of an axial fan rotor blade migrates radially outward and accumulates near the tip, increasing the near-tip blockage and loss. The radial outward migration of high-loss SS BL fluid is often interpreted in the literature as "outward centrifugation;" see, e.g., Refs. [3,12,15,19], dedicating the phenomenon to the dominance of centrifugal force over the radial pressure gradient.

Exceeding this simplistic interpretation, an analytical model has been elaborated upon for a detailed systematic investigation on the effects influencing the radial outward fluid migration in the SS BL. With the use of the analytical model, the significance of the effects influencing the outward migration has been quantified in an experiment-based case study. Such a quantification has been supplemented by examining the details of the measured flow field—see Figs. 3 and 4. On this basis, it has been concluded that the CVD ($d\psi_D/dR > 0$) tends to intensify the outward migration

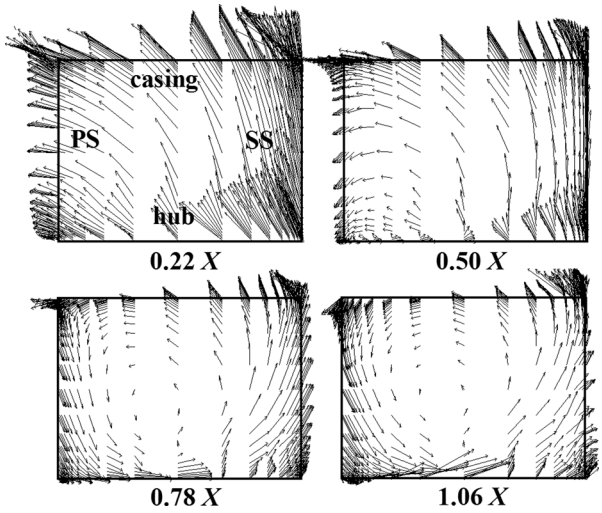

Fig. 2 Secondary flow vector diagrams for a CVD rotor [18] on planes normal to the rotational axis. The leading and trailing edges are at $X = 0$ and $X = 1$, respectively.

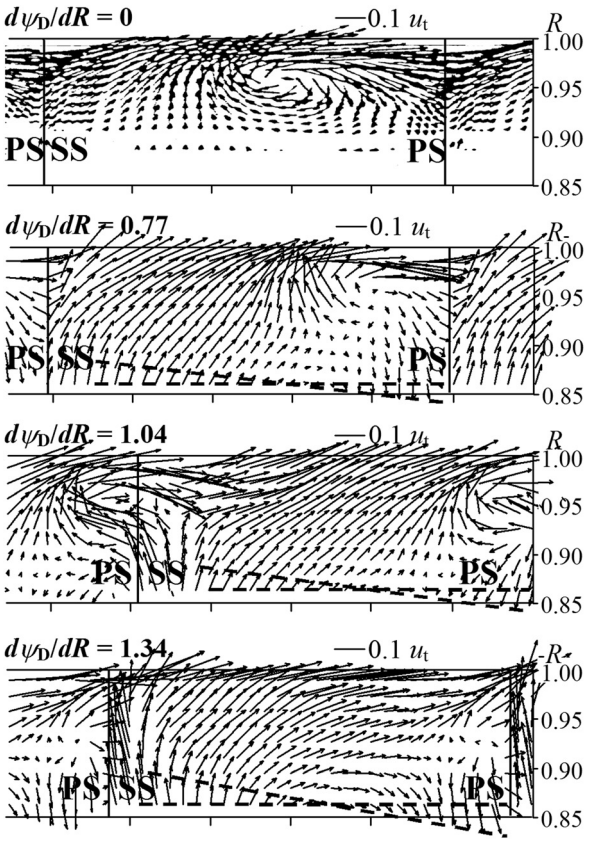

Fig. 3 Secondary flow vector plots for rotor exit planes

and near-tip accumulation of fluid in the SS BL, in comparison to the FVD ($d\psi_D/dR = 0$).

Such a tendency of the intensification of the SS BL fluid outward migration is related to the SS radially outward blade passage flow visualized in Fig. 2 and associated with the vortices shed from the CVD blade of $d\psi_D/dR > 0$. The intensification of the radially outward motion of the high-loss SS BL fluid, along with its stagnation near the tip increasing the endwall blockage, can be recognized in the diagrams presented in Figs. 3 and 4 [17] for comparative USW rotors of various $d\psi_D/dR$ values. The diagrams

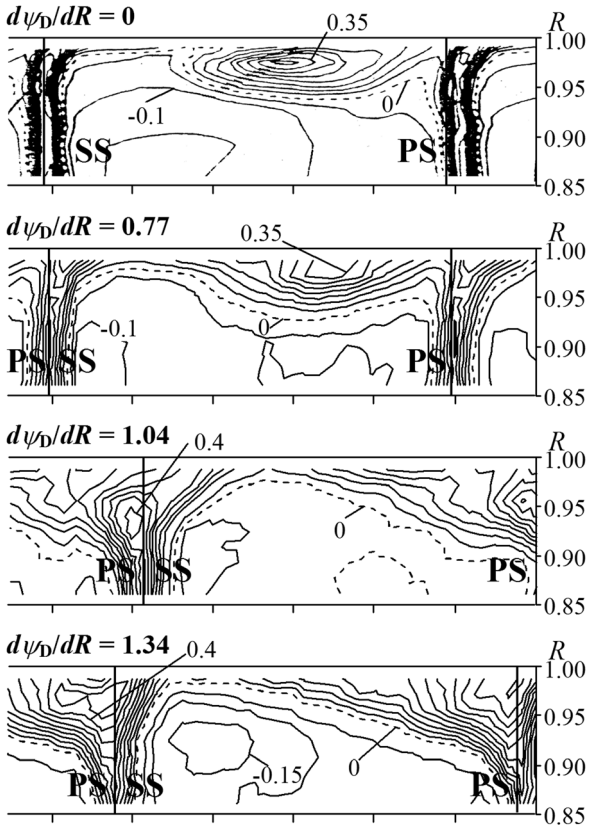

Fig. 4 Plots of the rotor exit relative kinetic energy defect coefficient ζ. Increment: 0.05.

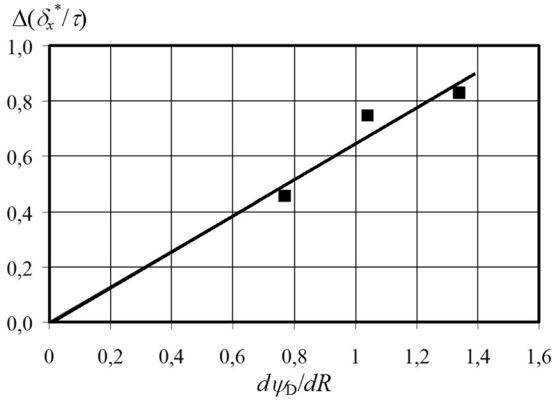

Fig. 5 Contribution of the effect of the spanwise changing blade circulation to the endwall blockage

in Figs. 3 and 4 are postprocessed from measurement data obtained close downstream of the trailing edges. The secondary flow velocity was obtained as a velocity component perpendicular to the design relative flow direction. The relative kinetic energy defect coefficient, suggesting the local loss, was defined as the difference between the designed and actual relative kinetic energy normalized by the designed relative kinetic energy. The data regions are transformed into identical rectangular domains in the figure. The plots present a pitchwise range of a 4/3 blade passage and a spanwise range of $R > 0.85$. Short vertical segments below the figures are drawn for every 20% of the blade pitch. The midline of the blade wake, characterized by a local maximum of the relative kinetic energy defect, is approximated by a vertical solid line. For the ζ plots, dashed contour lines indicate zero values. Figure 3 suggests that the radial velocity varies approximately linearly in the pitchwise direction for the CVD ($d\psi_D/dR > 0$) rotors.

The magnitude of the radial velocity, developing in association with the shed vortices, was found to be nearly proportional to $d\psi_D/dR$ *for the USW rotors*. This is illustrated by the angle between the dashed lines aligned with the starting and ending points of the secondary flow velocity vectors in Fig. 3. This angle slightly increases with $d\psi_D/dR$.

In Fig. 4, the loss appears to increase with $d\psi_D/dR$ in the blade wakes and in the tip vortex core (near the casing), overlapping with the zone of maximum intensity of the radially outward velocity. The preceding findings suggest that the radial outward flow on the SS due to CVD contributes to the losses near the tip, also generated in the loss core of the tip leakage vortex.

For quantifying the near-tip endwall blockage, the axial displacement thickness δ_x^* (see, e.g., Ref. [1]) has been calculated from the measurement data for USW rotors with tip clearance. As suggested in Refs. [20,21], the endwall blockage is influenced by the blade tip loading along with other parameters such as the inlet boundary layer, the clearance height, the stagger angle, the solidity, and the blade loading profile. In the view of the formerly discussed loss-increasing effect of the CVD near the tip, this parameter set has been supplemented with $d\psi_D/dR$ as a new parameter. Based on thee experiments, the approximate relationship presented in Fig. 5 [17] has been established. *In the case of the USW blades, the increment in the axial displacement thickness at the near-tip endwall due to the CVD is proportional to* $d\psi_D/dR$. This relationship can be utilized in the preliminary blade design.

The beneficial effect of the FSW, by moderating the outward migration and near-tip accumulation of high-loss SS BL fluid, is explained in the literature (see, e.g., Refs. [1,12,15,19]) using the following verbally expressed intuitive model, presented in Fig. 6. By sweeping the blade forward, the isobar lines in the decelerating zone of the blade SS are inclined in the forward direction, following the inclination of the stacking line. This results in an additional radial pressure gradient acting against the outward migration. Exceeding this verbally expressed intuitive model, such a benefit of the FSW has been confirmed by the purposeful application of the aforementioned analytical model. As previously pointed out, the *CVD tends to promote the radial outward migration and near-tip stagnation of the SS BL fluid, in comparison to the FVD*. Keeping this in mind, the following conclusion has been drawn. *The benefit of the FSW, in terms of moderating the near-tip loss and blockage, is expected to be better utilized for the rotors of the CVD, in comparison to the FVD. The more the* $d\psi_D/dR$ *parameter, the more the benefit expected from the FSW of the appropriate* $|\lambda|$. Such a benefit is demonstrated, e.g., in Ref. [1], in terms of the retardation of the outward migration of low-energy fluid on the suction side and the moderation of the

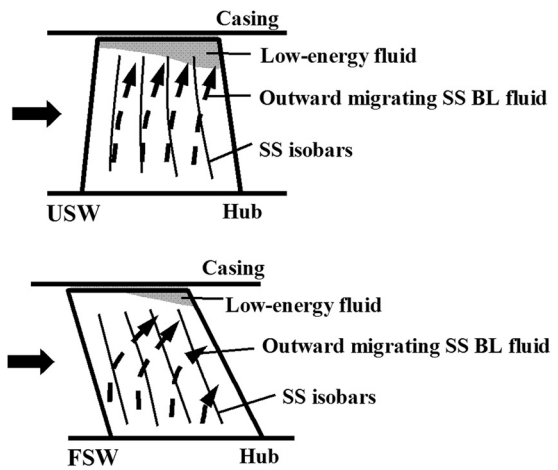

Fig. 6 Sketch of the suppression of the radially outward flow of the SS BL fluid by means of the FSW

endwall blockage and the associated losses. The data in [22] indicate that, in the region of $R > 0.92$ (including the endwall BL), the mass-averaged total pressure loss reduction due to the FSW is approximately 2% of the dynamic pressure calculated with the inlet relative velocity at midspan.

Loss Farther Away From the Endwalls

This section discusses the effects of the CVD, along with the effect of its combination with the FSW, on the total pressure loss developing farther away from the annulus walls. The discussion presented herein is reported in detail in Ref. [23].

The literature data on diffuser flows of various levels of complexity were postprocessed and evaluated in a comprehensive manner in comparative case studies. The studies incorporated two-dimensional (2D) rectilinear blade cascade flows and 3D annular rotor blade cascade flows. The inlet and outlet geometrical and velocity conditions were considered as fixed for each comparative study. The following common conclusions, being valid for each type of examined flow, have been drawn. In decelerating flows, the consequence of decreasing the flow path length along the wall is to decrease the total pressure loss—due to moderating the effect of wall skin friction—provided that the adverse streamwise pressure gradient remains below a critical value. In contrast, increasing the flow path length leads to an increase of the total pressure loss, via increasing the effect of wall skin friction, in the same range of the subcritical pressure gradient.

In the discussion that follows, the decelerating flow region over the SS blade surface is examined, in which the majority of loss is generated farther away from the endwalls (see, e.g., Refs. [3,24]).

The preceding conclusions are illustrated herein with the use of 2D cascade data published by Lieblein [25]. The Lieblein data have been postprocessed in order to deduce the variance of total pressure loss with the cascade solidity c/s. For the prescribed blade spacing s, the solidity determines the blade chord length c, representing the "blade wetted" [24] length, i.e., the flow path length along which the fluid particles are exposed to wall skin friction in the 2D cascade flow under discussion. Examples for the postprocessed Lieblein data are given in Fig. 7 [23]. It is visible in the figure that, for the prescribed inlet and outlet flow angles α_1 and α_2, reducing the solidity c/s, i.e., reducing the flow path length at fixed spacing s, leads to the decrease of the total pressure loss coefficient ω, until a loss minimum of ω_{min}, which is associated with a critical (allowed maximum) pressure gradient, is reached. In contrast, ω increases with the solidity in the same solidity range.

Such postprocessing of the 2D cascade data offers a preliminary design tool for predicting in which solidity range and in what order of magnitude one may expect a loss reduction by reducing the actual flow path length, i.e., by reducing the "effective blade chord length" [26], for prescribed inlet and outlet flow angles and fixed blade spacing. The existence of ω_{min} manifests the existence of optimum solidity, allowing for minimum loss. The existence of optimum solidity has already been suggested in [25]. Determining optimum solidity on the basis of 2D cascade correlations is an objective of preliminary blade design, e.g., [27].

The preceding concept of viewing the total pressure loss as being dependent on the flow path length has been extended to 3D rotor flows as follows.

The development of the radial flow introduces three-dimensionality in the flow paths along the SS. Such 3D flow paths become elongated, in comparison to the "idealistic" 2D through-flow, as pointed out, e.g., in Refs. [26,28]. In Ref. [26], the intensification of the radial outward flow was reported to increase the "effective chord length," i.e., the length of elongated 3D flow paths over the blade surface. As Ref. [28] presents, the 3D streamlines indicate a longer trajectory of the particles over the SS, which was found to increase the BL thickness (associated with the increased loss).

In the view that the CVD results in the intensification of the radially outward flow in the SS BL [17], the following conclusion has been drawn. *In comparison to the FVD, the CVD applied to the USW axial flow rotor blades tends to represent an additional source of total pressure loss farther away from the endwalls. The cause is the elongation of the flow paths along the SS—and thus, increase of effect of the wall skin friction—due to the intensified radial outward flow. The more the* $d\psi_D/dR$ *parameter, the more the elongation of the flow paths and the associated additional loss expected.* The elongation of the flow paths due to the CVD, in comparison to the "idealistic" 2D through-flow, is schematically shown on the USW rotor in Fig. 8 [23].

This adverse effect can be moderated by the incorporation of the FSW in the CVD rotor geometry, via shortening the flow paths on the suction side, while retaining the inlet and outlet velocity conditions. Such an effect is illustrated in Fig. 8, comparing the USW and the FSW rotors of an identical 2D chord. The concept is supported by Refs. [4,29], outlining the fact that the FSW severely limits the range of the radial travel of the BL fluid by truncating the flow path near the trailing edge. Upon this basis, the following statement has been formulated. *The benefit of the FSW, in terms of moderating loss away from the endwalls, is expected to be better utilized for the rotors of the CVD, in comparison to the FVD. The*

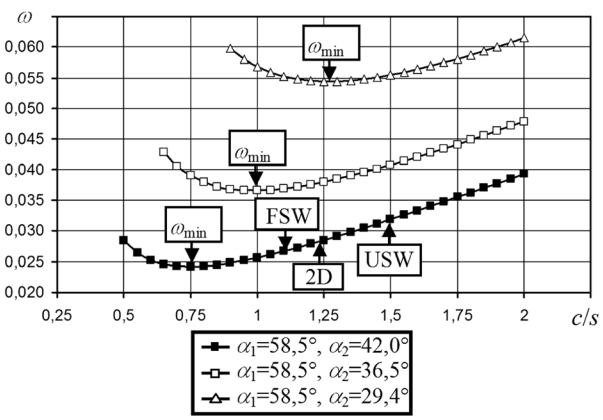

Fig. 7 Examples for the variance of the total pressure loss with blade solidity

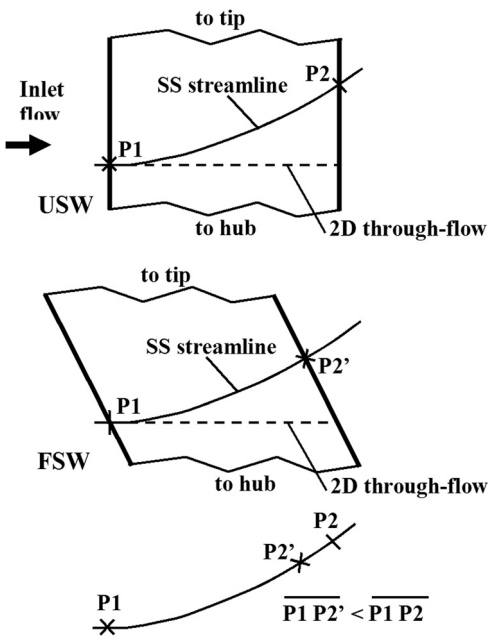

Fig. 8 Flow path-elongating effect due to the CVD; shortening of the flow path by means of the FSW

more the $d\psi_D/dR$ parameter, the more the benefit expected from the FSW of the appropriate $|\lambda|$. This statement adds to the findings in the previous section, also discussing the special benefits of the FSW applied to the CVD rotors, but only in moderating loss *near the tip*.

The findings previously outlined are illustrated in the following CFD-based case study [1]. Figure 9 (adapted from Ref. [1], in Ref. [23]) presents the CFD plots on the comparative USW and FSW rotors of the CVD. The rotors have an identical midspan solidity. The solidity corresponding to the 2D midspan chord, assuming an idealistic 2D through-flow along a cylindrical stream surface, is 1.235. The data point corresponding to this solidity and related to the inlet and outlet flow angles of the case study rotors is marked in Fig. 7, using the label "2D." Figure 9 shows the static pressure contours and limiting streamlines over the suction surfaces, which are plotted in their meridional views. The limiting streamlines under the present discussion, passing the SS at near-midspan and near-midchord, are marked with bold lines. The inlet and outlet flow angles at the near-leading edge and near-trailing edge streamline sections are nearly identical for the two rotors [30] (at midspan, $\alpha_1 = 58.5$ deg, $\alpha_2 = 42$ deg). Furthermore, the spanwise blade circulation gradient is nearly identical for the two rotors in the near-midspan zone [30]: $d\psi_D/dR = 1.04$. The dominant portion of the scrutinized flow paths proceeds through the blade passages away from the endwalls. Near-endwall loss-generating effects can be clearly distinguished from the loss zone developing along the blade surface farther away from the annulus walls, as can be seen in the loss coefficient plots in Fig. 10.

As can be seen in Fig. 9 with a single glance, the CVD concept in the case of the USW rotor results in a significantly elongated 3D flow path compared to the 2D through-flow. Such a 3D "effective chord" [26] of the USW is ≈20% longer than the 2D midspan chord (corresponding to the fictitious 2D through-flow along a cylindrical stream surface). In the FSW case, however, the radial outward flow developing due to the CVD concept has been

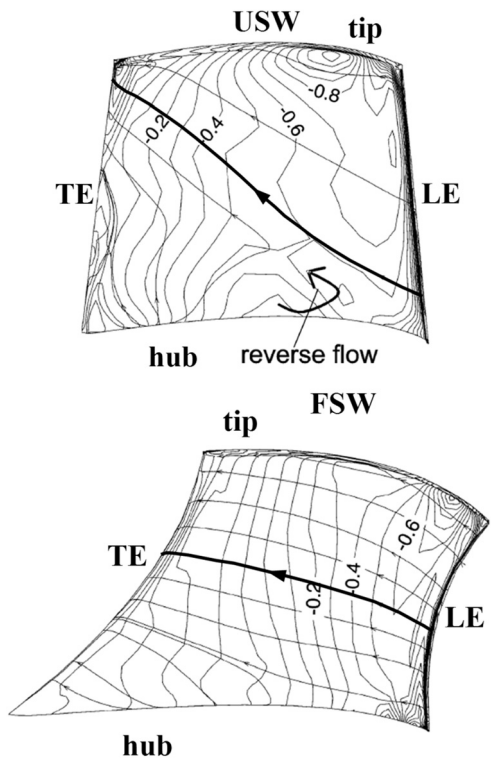

Fig. 9 Computed static pressure coefficient C_p distribution and limiting streamlines on the USW and FSW blades on the SS (adapted from Ref. [1]). The studied flow paths are indicated with bold lines. (LE and TE: leading and trailing edges.)

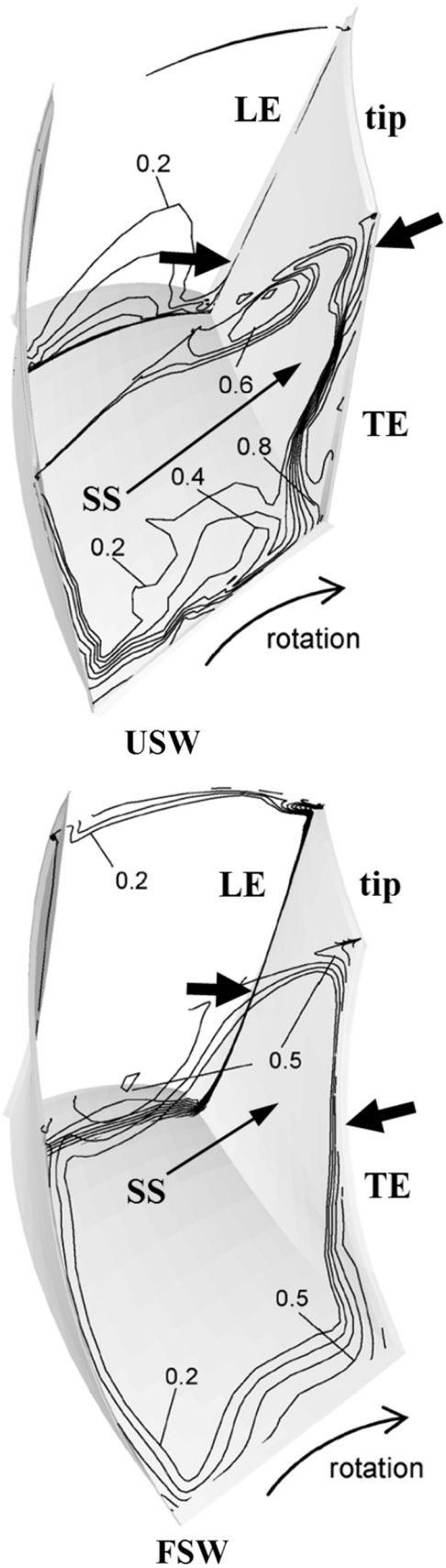

Fig. 10 Evolution of the total pressure loss coefficient inside the blade passages at 10% and 98% blade chord (adapted from Ref. [1]). Bold arrows: location of the entrance and exit of the studied flow paths. (LE and TE: leading and trailing edges.)

attenuated due to the FSW, as expected on the basis of the previous section. The FSW flow path is spectacularly shorter than the USW one. Such a 3D "effective chord" of the FSW is ≈10% shorter than the 2D midspan chord. Therefore, a reduction of the ≈30% 2D midspan chord has been achieved in the length of the 3D "effective chord," with the introduction of the FSW. Calculated with the midspan blade spacing, the solidities corresponding to these 3D "effective chords" are indicated in Fig. 7, using the labels "USW" and "FSW". Figure 7 forecasts that reducing the 3D "effective chord" with the use of the FSW still keeps the streamwise adverse pressure gradient in the subcritical range: the solidities are above the solidity related to ω_{min}. Furthermore, an ≈15% reduction of ω is predicted using the figure, due to the incorporation of the FSW.

Figure 10 (adapted from Ref. [1], in Ref. [23]) presents the evolution of the computed total pressure loss inside the blade passages, showing the contours of the local total pressure loss coefficient [23] at the 10% and 98% midspan chord positions. The loss reduction in the near-tip region of the SS BL due to the FSW, related to the discussion in the previous section, is visible in the figure. The entry and exit spanwise locations of the scrutinized SS flow paths, shown in Fig. 9 using bold lines, are indicated near the leading edges and trailing edges by bold arrows in Fig. 10. The reduction of the loss (BL thinning) over the SS is due to the shortening of the studied flow path due to the FSW. The BL thinning is also visible for the FSW in the vicinity of the studied flow path along the span, in which region a systematic shortening of flow paths can be observed in Fig. 9. The spanwise mean value of loss reduction due to FSW is approximately 10% of the dynamic pressure calculated with the inlet relative velocity at midspan [22].

CVD: Influence of Spanwise Circulation Distribution Due to FSW

As the previous sections suggest, the parameter $d\psi_D/dR$, representing the intensity of spanwise variation of design blade circulation, is a key feature of the influence of the CVD on the 3D interblade flow features. In classic preliminary blade design, the blade is designed for a prescribed CVD swirl distribution, and sweep is introduced afterwards, independently from the CVD method. The blade is recommended to be corrected for nonradial stacking, in order to achieve the prescribed total pressure rise, while retaining the favorable aerodynamic features of sweep [9]. As an aid to the designer prior to sweep correction, it is examined herein how the circulation gradient originally prescribed for the USW blading tends to change when introducing sweep without correction. In these studies, reports were overviewed on swept rotors for which no sweep correction has been applied; see, e.g., Refs. [11–14,28,31–37].

As suggested in Ref. [9], in the absence of sweep correction, the spanwise circulation distribution is influenced by sweep via two mechanisms.

(a) *The modification of the rotor inlet flow due to positive sweep*. Sweep is positive(negative) near the endwall when a blade section under consideration is upstream(downstream) of the adjacent inboard section. Therefore, positive(negative) sweep appears at the tip(hub) of a FSW blade. It has been outlined in Ref. [9] that the near-endwall sections of positive sweep protrude into the upstream relative flow field and exhibit work on the fluid in advance, compared to the inboard (more downstream) blade sections. This was found to result in locally increased inlet axial velocity, as the data, e.g., in [21,31–33,38,39] suggest. At a prescribed design flow rate, an increase of the inlet axial velocity near the positively swept tip of the FSW is associated with the reduction of the axial velocity inlet to the inboard sections. This results in an increased incidence angle (measured from the axial direction), corresponding to an increased load of the inboard blade sections. Therefore, the FSW blade tip causes the uploading of blade sections at lower radii.

(b) *The modification of the blade section load due to sweep near the endwalls*. In addition to the aforementioned mechanism, positive sweep near the tip of the FSW blade causes the local unloading of the blade [7,8,31,37,40,41]. Furthermore, if the FSW extends to the entire span, it corresponds to negative sweep near the hub, causing uploading of the blade sections in the near-hub region (additionally to the uploading described in the previous paragraph).

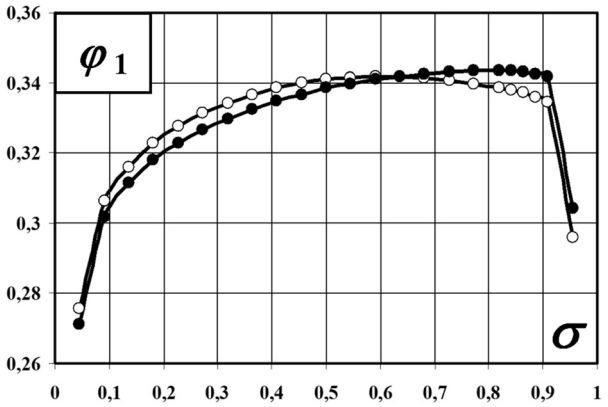

Fig. 11 Computed inlet axial velocity profiles along the span. White dots: USW. Black dots: FSK.

For an example of rotor inlet flow modification, Fig. 11 [11] is presented herein. The local blade loading is represented by ψ. Figure 12 gives examples for the modification of $\psi(R)$ due to

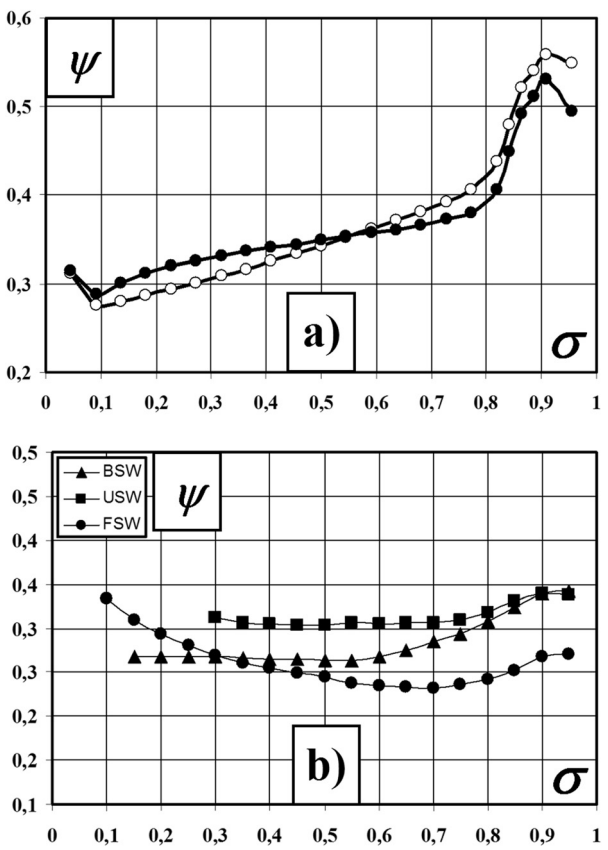

Fig. 12 Isentropic total pressure rise distributions along the span. (*a*) Computations [11]. White dots: USW. Black dots: FSK. (*b*) Measurements [36].

sweep. Figures 11 and 12(*a*) [11] present the effect of the FSK applied to the upper half-span only. Figure 12(*b*) [36] shows the $\psi(R)$ distributions for applying a backward sweep ($\lambda = 45$ deg, "BSW"), no sweep ($\lambda = 0$ deg, "USW"), and the FSW ($\lambda = -45$ deg) to a rotor of the FVD. It is visible that by sweeping the blade "more and more forward" (BSW → USW → FSW), the blade sections toward the tip tend to be unloaded, and the sections toward the hub tend to be uploaded. This results in the moderation of $d\psi_D/dR$ in the sequence of "BSW" → "USW" → "FSW."

The findings discussed in this section can be summarized as follows. *In the absence of sweep correction, increasing the FSW angle $|\lambda|$ and increasing the extension of the FSW from the tip toward the lower radii tends to reduce $d\psi/dR$ away from the endwalls. By such means, the originally intended CVD blade circulation distribution tends toward a free-vortex pattern.* Such an effect is to be considered in design refinement.

Summary

The qualitative trends established herein for low-speed axial fan rotors at the design flow rate are summarized as follows and are illustrated in Figs. 13 and 14. In the figures, the flow away from the endwalls is represented by only a single streamline passing the SS at midspan and midchord (indicated with a bold line) for clarity.

(1) Due to spanwise changing blade circulation represented by $d\psi_D/dR > 0$, vortices are shed from the CVD blade. These vortices are associated with the radially outward flow on the SS. Therefore, the CVD tends to intensify the radially outward flow on the SS, in comparison to the FVD. For the USW rotors investigated, the magnitude of the radial velocity due to the CVD was found to be nearly proportional to $d\psi_D/dR$.

(2) In the case of the USW blades, the adverse effect of the intensification of the SS radially outward flow due to the CVD (Point 1), in comparison to the FVD, is twofold (Fig. 13):

(2a) The radially outward migration and near-tip stagnation of the SS BL fluid tends to intensify, leading to increased near-tip loss and blockage. In the case of the USW blades, the increment in the axial displacement thickness at the near-tip endwall due to the CVD was found to be proportional to $d\psi_D/dR$.

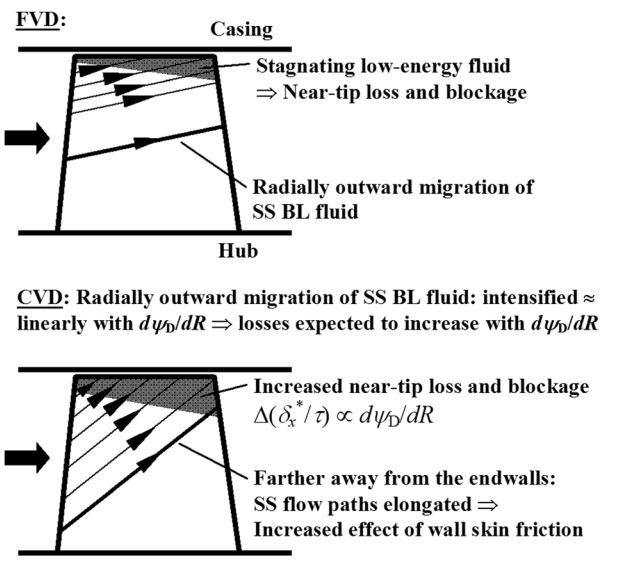

Fig. 13 The USW rotors of the FVD versus the CVD: comparison of the SS phenomena

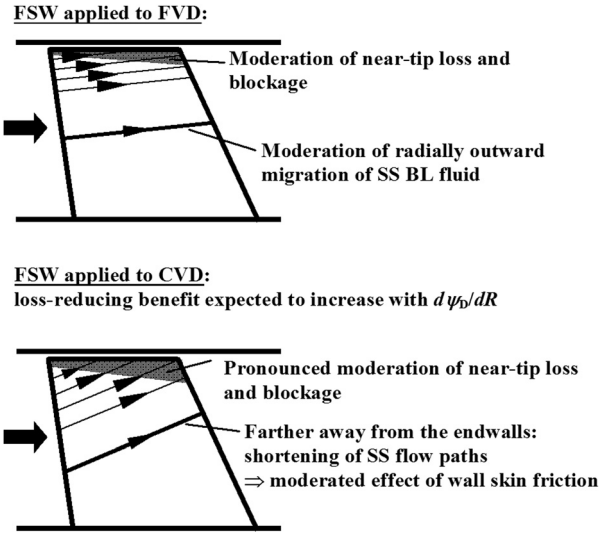

Fig. 14 Applying the FSW to the rotors of the FVD versus the CVD: comparison of the SS phenomena

(2b) Farther away from the endwalls, the 3D flow paths are elongated on the SS and, for this reason, the effect of the wall skin friction increases. The more the $d\psi_D/dR$ parameter, the more the elongation of the flow paths and the associated additional loss expected.

Based on Points (2a) and (2b), the CVD tends to represent additional sources of loss near the tip and further away from the endwalls, in comparison to the FVD, in the case of the USW blades. The more the $d\psi_D/dR$, the more the additional losses expected.

(3) The FSW applied to the rotors of the CVD appears as a unique remedial strategy against the adverse effects outlined in Point 2, while retaining the beneficial features of the CVD. Applying the FSW to the rotors of the CVD tends to represent additional benefits in comparison to applying it to the FVD rotors, via moderation of the already intensified radially outward flow on the SS (Point 1). The additional benefits are twofold:

(3a) The intensified near-tip loss and blockage (Point 2a) offers a basis for a more spectacular loss and blockage reduction via the FSW.

(3b) Further away from the endwalls, the already elongated 3D flow paths on the SS (Point (2b)) can be shortened using the FSW, thus moderating the effect of the wall skin friction. The shortening of flow paths is partly due to:

- an aerodynamic feature of the FSW, i.e., moderation of the radially outward flow, and partly due to
- a geometrical feature of the FSW, i.e., truncating the available SS flow paths near the trailing edge

Based on Points (3a) and (3b), the benefit of the FSW is expected to be better utilized in the case of the CVD, in comparison to the FVD, for the reduction of losses near the tip and further away from the endwalls. The more the $d\psi_D/dR$, the more the loss reduction expected from the FSW of the appropriate $|\lambda|$ and sweep correction.

(4) In the absence of sweep correction, the originally intended CVD blade circulation distribution is modified along the entire span due to the FSW, via the following effects:

(4a) modification of the incidence due to positive sweep near the tip

(4b) modification of the load of the blade sections due to sweep, from midspan toward the endwalls

In accordance with Points (4a) and (4b), in the absence of sweep correction, increasing the FSW angle $|\lambda|$ and increasing the extension of the FSW from the tip toward the lower radii tends to reduce $d\psi/dR$ away from the endwalls. By such means, the originally intended CVD blade circulation distribution tends toward a free-vortex pattern. This tends to result in moderating the contribution of the blade sections at higher radii to rotor performance; thus reducing the global total pressure rise. The preceding draws attention to the importance of sweep correction when applying the FSW to the rotors of the CVD.

The preceding *qualitative* guidelines give aid to the designer in the preliminary judgment of the 3D interblade effects expected in the CVD and in the CVD incorporating the FSW. However, it is not expected to be possible to develop generally valid simplified rules for *quantification* of the aforementioned effects. The harmonization of the $\psi(R)$ and $|\lambda|$ (R) distributions and sweep correction must rely on a suitable CFD technique in a particular design assignment. Some examples for CFD techniques proven to appropriately resolve the combined CVD and FSW effects are as follows: commercially available software (e.g., ANSYS FLUENT [10,11]), along with in-house developed codes (e.g., Ref. [1].). In Ref. [42], the author proposes a CFD-aided method for systematic incorporation of FSW in the preliminary CVD of axial flow rotors.

The pronounced loss-reducing benefit of the FSW applied to rotors of the CVD is supported by the following latent tendency, which is observed in the literature and summarized in the studies by the author in Ref. [9]. In these studies, the FSW was found to be beneficial in terms of an efficiency gain up to 3% [1] at the design point, when applied to the CVD rotors; see, e.g., Refs. [1,12,14,38,43]. However, when applying the FSW to the FVD rotors; see, e.g., Refs. [21,28,34–37,44], the efficiency gain was either less (maximum efficiency gain up to 2% in [21]), or even efficiency deterioration was observed at the design flow rate.

The special benefit of the FSW applied to the rotors of the CVD is in agreement with the viewpoint in [16]. Here, the authors suggest that only modest aerodynamic improvement can be achieved by the FSW for fan bladings of moderate load, low solidity, and FVD. They expect more significant benefits of the FSW in the presence of stronger nonfree vortex flow, i.e., for fans of the CVD.

Acknowledgment

This work has been supported by the Hungarian National Fund for Science and Research under Contract No. OTKA K 83807.

Nomenclature

Latin Letters

c = blade chord length
C_p = static pressure coefficient (local static pressure, minus pitch-averaged mean static pressure at inlet at midspan, divided by $\rho\, u_t^2/2$)
R = radius normalized by tip radius
s = blade spacing
u_t = blade tip circumferential velocity
X = fraction of axial chord

Greek Letters

α_1, α_2 = inlet and outlet relative flow angles, from axial direction
δ_x^* = axial displacement thickness
$\Delta(\delta_x^*/\tau)$ = increment in endwall blockage related to $d\psi_D/dR$
ζ = relative kinetic energy defect coefficient
λ = sweep angle
ρ = fluid density
σ = fraction of span
τ = tip clearance
φ_1 = local inlet axial flow coefficient (pitchwise area-averaged inlet axial velocity divided by u_t)
Φ = global flow coefficient (annulus area-averaged axial velocity divided by u_t)
ψ = local isentropic total pressure rise coefficient (pitchwise mass-averaged isentropic total pressure rise divided by $\rho u_t^2/2$)
Ψ = global total pressure coefficient (annulus mass-averaged total pressure rise divided by $\rho u_t^2/2$)
ω = total pressure loss coefficient

Subscript

D = design point; at the design flow rate

Acronyms

BL = blade boundary layer
BSW = blade backward sweep
CFD = computational fluid dynamics
CVD = controlled vortex design
FSK = circumferential forward skew
FSW = blade forward sweep
FVD = free vortex design
SS = blade suction side
USW = unswept
2D = two-dimensional (flow)
3D = three-dimensional (flow)

References

[1] Corsini, A., and Rispoli, F., 2004, "Using Sweep to Extend the Stall-Free Operational Range in Axial Fan Rotors," Proc. Inst. Mech. Eng., Part A, **218**, pp. 129–139.
[2] Cyrus, V., and Wurst, P., 2011, "High Pressure Axial Flow Fans for Power Industry," Proceedings of the 9th European Conference on Turbomachinery Fluid Dynamics and Thermodynamics, Istanbul, Turkey, March 21–25, pp. 81–93.
[3] Lakshminarayana, B., 1996, *Fluid Dynamics and Heat Transfer of Turbomachinery*, John Wiley & Sons, Inc., New York.
[4] Carolus, T., 2003, *Ventilatoren*, Teubner, Leipzig, Germany.
[5] Bianchi, S., Corsini, A., Rispoli, F., and Sheard, A. G., 2008, "Experimental Aeroacoustic Studies on Improved Tip Geometries for Passive Noise Signature Control in Low-Speed Axial Fans," ASME Paper No. GT2008-51057.
[6] Sarraf, C., Nouri, H., Ravelet, F., and Bakir, F., 2011, "Experimental Study of Blade Thickness Effects on the Overall and Local Performances of a Controlled Vortex Designed Axial-Flow Fan," Exp. Therm. Fluid Sci., **35**, pp. 684–693.
[7] Gallimore, S. J., Bolger, J. J., Cumpsty, N. A., Taylor, M. J., Wright, P. I., and Place, J. M. M., 2002, "The Use of Sweep and Dihedral in Multistage Axial Flow Compressor Blading: Part I—University Research and Methods Development," ASME J. Turbomach., **124**(4), pp. 521–532.
[8] Gallimore, S. J., Bolger, J. J., Cumpsty, N. A., Taylor, M. J., Wright, P. I., and Place, J. M. M., 2002, "The Use of Sweep and Dihedral in Multistage Axial Flow Compressor Blading—Part II: Low and High-Speed Designs and Test Verification," ASME J. Turbomach., **124**(4), pp. 533–541.
[9] Vad, J., 2008, "Aerodynamic Effects of Blade Sweep and Skew in Low-Speed Axial Flow Rotors Near the Design Flow Rate: An Overview," Proc. Inst. Mech. Eng., Part A, **222**, pp. 69–85.
[10] Vad, J., Horváth, Cs., Lohász, M. M., Jesch, D., Molnár, L., Koscsó, G., Nagy, L., Dániel, I., and Gulyás, A., 2011, "Redesign of an Electric Motor Cooling Fan for Reduction of Fan Noise and Absorbed Power," Proceedings of the 9th European Conference on Turbomachinery Fluid Dynamics and Thermodynamics, Istanbul, Turkey, March 21–25, pp. 69–79.
[11] Vad, J., Kwedikha, A. R. A., Horváth, Cs., Balczó, M., Lohász, M. M., and Régert, T., 2007, "Aerodynamic Effects of Forward Blade Skew in Axial Flow Rotors of Controlled Vortex Design," Proc. Inst. Mech. Eng., Part A, **221**, pp. 1011–1023.
[12] Yamaguchi, N., Tominaga, T., Hattori, S., and Mitsuhashi, T., 1991, "Secondary-Loss Reduction by Forward-Skewing of Axial Compressor Rotor Blading," Proceedings of the Yokohama International Gas Turbine Congress, Yokohama, Japan, October 27–November 1, pp. 61–68.
[13] Beiler, M. G., and Carolus T. H., 1999, "Computation and Measurement of the Flow in Axial Flow Fans With Skewed Blades," ASME J. Turbomach., **121**, pp. 59–66.
[14] Li, Y., Quang, H., and Du, Z.-H., 2007, "Optimization Design and Experimental Study of Low-Pressure Axial Fan With Forward-Skewed Blades," Int. J. Rotating Mach., 2007, p. 85275.

[15] Govardhan, M., Krishna Kumar, O. G., and Sitaram, N., 2007, "Computational Study of the Effect of Sweep on the Performance and Flow Field in an Axial Flow Compressor Rotor," Proc. Inst. Mech. Eng., Part A, **221**, pp. 315–329.
[16] Cros, S., and Carbonneau, X., 2009, "Computational Study of the Aerodynamic Impact of Stall Margin Improvements in a High Tip Speed Fan," Proceedings of the 8th European Conference on Turbomachinery Fluid Dynamics and Thermodynamics, Graz, Austria, March 23–27, pp. 401–410.
[17] Vad, J., 2010, "Radial Fluid Migration and Endwall Blockage in Axial Flow Rotors," Proc. Inst. Mech. Eng., Part A, **224**, pp. 399–417.
[18] Corsini, A., 1999, private communication.
[19] Ramakrishna, P. V., and Govardhan, M., 2011, "On Loading Corrections and Loss Distributions in Low-Speed Forward Swept Axial Compressor Rotors," Proc. Inst. Mech. Eng., Part A, **225**, pp. 120–130.
[20] Khalid, S. A., Khalsa, A. S., Waitz, I. A., Tan, C. S., Greitzer, E. M., Cumpsty, N. A., Adamczyk, J. J., and Marble, F. E., 1999, "Endwall Blockage in Axial Compressors," ASME J. Turbomach., **121**, pp. 499–509.
[21] McNulty, G. S., Decker, J. J., Beacher, B. F., and Khalid, S. A., 2003, "The Impact of Forward Swept Rotors on Tip-Limited Low-Speed Axial Compressors," ASME Paper No. GT2003-38837.
[22] Corsini, A., and Rispoli, F., 2003, "The Role of Forward Sweep in Subsonic Axial Fan Rotor Aerodynamics at Design and Off-Design Operating Conditions," ASME Paper No. GT2003-38671.
[23] Vad, J., 2011, "Correlation of Flow Path Length to Total Pressure Loss in Diffuser Flows," Proc. Inst. Mech. Eng., Part A, **225**, pp. 481–496.
[24] Pullan, G., and Harvey, N. W., 2007, "Influence of Sweep on Axial Flow Turbine Aerodynamics at Midspan," ASME J. Turbomach., **129**, pp. 591–598.
[25] Lieblein, S., 1965, "Experimental Flow in Two-Dimensional Cascades," *Aerodynamic Design of Axial-Flow Compressors*, NASA SP-36, NASA, Washington DC.
[26] Gifford, N. L., Savory, E., and Martinuzzi, R. J., 2007, "Experimental Study of Automotive Cooling Fan Aerodynamics," SAE Paper No. 2007-01-1525.
[27] Rossetti, A., Ardizzon, G., Pavesi, G., and Cavazzini, G., 2010, "An Optimum Design Procedure for an Aerodynamic Radial Diffuser With Incompressible Flow at Different Reynolds Numbers," Proc. Inst. Mech. Eng., Part A, **224**, pp. 69–84.
[28] Helming, K., 1996, "Numerical Analysis of Sweep Effects in Shrouded Propfan Rotors," J. Propul. Power, **12**, pp. 139–145.
[29] Wright, T., and Simmons, W. E., 1990, "Blade Sweep for Low-Speed Axial Fans," ASME J. Turbomach., **112**, pp. 151–158.
[30] Corsini, A., Rispoli, F., Vad, J., and Bencze, F., 2001, "Effects of Blade Sweep in a High Performance Axial Flow Rotor," Proceedings of the 4th European Conference on Turbomachinery Fluid Dynamics and Thermodynamics, Florence, Italy, March 20–23, pp. 63–76.
[31] Kuhn, K., 2000, "Experimentelle Untersuchung einer Axialpumpe und Rohrturbine mit gepfeilten Schaufeln," Ph.D. dissertation, Technische Universität Graz, Institut for Hydraulische Strömungsmaschinen, Graz, Austria.
[32] Forstner, M., Kuhn, K., Glas, W., and Jaberg, H., 2001, "The Flow Field of Pump Impellers With Forward and Backward Sweep," Proceedings of the 4th European Conference on Turbomachinery Fluid Dynamics and Thermodynamics, Florence, Italy, March 20–23, pp. 577–587.
[33] Forstner, M., 2002, "Experimentelle Untersuchungen an vorwärts und rückwärts gepfeilten Axialpumpenschaufeln," Ph.D. dissertation, Technische Universität Graz, Institut for Hydraulische Strömungsmaschinen, Graz, Austria.
[34] Rohkamm, H., Wulff, D., Kosyna, G., Saathoff, H., Stark, U., Gümmer, V., Swoboda, M., and Goller, M., 2003, "The Impact of Rotor Tip Sweep on the Three-Dimensional Flow in a Highly-Loaded Single-Stage Low-Speed Axial Compressor: Part II—Test Facility and Experimental Results," Proceedings of the 5th European Conference on Turbomachinery Fluid Dynamics and Thermodynamics, Prague, Czech Republic, March 18–21, pp. 175–185.
[35] Clemen, C., Gümmer, V., Goller, M., Rohkamm, H., Stark, U., and Saathoff, H., 2004, "Tip-Aerodynamics of Forward-Swept Rotor Blades in a Highly-Loaded Single-Stage Axial-Flow Low-Speed Compressor," Proceedings of the 10th International Symposium on Transport Phenomena and Dynamics of Rotating Machinery (ISROMAC10), Honolulu, Hawaii, March 7–11, Paper No. 027.
[36] Vad, J., Kwedikha, A. R. A., and Jaberg, H., 2004, "Influence of Blade Sweep on the Energetic Behavior of Axial Flow Turbomachinery Rotors at Design Flow Rate," ASME Paper No. GT2004-53544.
[37] Vad, J., Kwedikha, A. R. A., and Jaberg, H., 2006, "Effects of Blade Sweep on the Performance Characteristics of Axial Flow Turbomachinery Rotors," Proc. Inst. Mech. Eng., Part A, **220**, pp. 737–751.
[38] Meixner, H. U., 1995, "Vergleichende LDA-Messungen an ungesichelten und gesichelten Axialventilatoren," Ph.D. dissertation, Universität Karlsruhe, VDI-Verlag, Reihe 7: Strömungstechnik, No. 266, Düsseldorf, Germany.
[39] Lee, G. H., Baek, J. H., and Myung, H. J., 2003, "Structure of Tip Leakage Flow in a Forward-Swept Axial-Flow Fan," Flow, Turbul. Combust., **70**, pp. 241–265.
[40] Denton, J. D., and Xu, L., 1999, "The Exploitation of 3D Flow in Turbomachinery Design," Turbomachinery Design Systems (Lecture Series 1999-02), Von Karman Institute for Fluid Dynamics, Sint-Genesius-Rode, Belgium.
[41] Clemen, C., and Stark, U., 2003, "Compressor Blades With Sweep and Dihedral: A Parameter Study," Proceedings of the 5th European Conference on Turbomachinery Fluid Dynamics and Thermodynamics, Prague, Czech Republic, March 18–21, pp. 151–161.
[42] Vad, J., 2012, "Incorporation of Forward Blade Sweep in Preliminary Controlled Vortex Design of Axial Flow Rotors," Proc. Inst. Mech. Eng., Part A, **226**(4), pp. 462–478.
[43] Beiler, M. G., 1996, "Untersuchung der dreidimensionalen Strömung durch Axialventilatoren mit gekrümmten Schaufeln," Ph.D. dissertation, Universität-GH-Siegen, VDI Verlag, Reihe 7: Strömungstechnik, No. 298, Düsseldorf, Germany.
[44] Rohkamm, H., Kosyna, G., Saathoff, H., and Stark, U., 2005, "Enhancement of Highly-Loaded Axial Compressor Stage Performance Using Rotor Blade Tip Tailoring, Part II—Experimental Results," Proceedings of the 6th European Conference on Turbomachinery Fluid Dynamics and Thermodynamics, Lille, France, March 7–11, pp. 100–110.